EFFECTS OF REYNOLDS NUMBER, BAFFLE ANGLE, AND BAFFLE DISTANCE ON 3-D TURBULENT FLOW AND HEAT TRANSFER IN A CIRCULAR PIPE

by

Oguz TURGUT** and Erkan KIZILIRMAK

Department of Mechanical Engineering, Faculty of Engineering, Gazi University, Maltepe, Ankara, Turkey

Original scientific paper
DOI:10.2298/TSCI121011045T

In this study, steady-state 3-D turbulent forced convection flow and heat transfer characteristics in a circular pipe with baffles attached inside pipe have been numerically investigated under constant wall heat flux boundary condition. Numerical study has been carried out for Reynolds number of 3000-50,000, Prandtl number of 0.71, baffle distances s/D of 1, 2, and 3, and baffle angle α of 30°-150°. Ansys Fluent 12.0.1 software has been used to solve the flow field. It is observed that circular pipe having baffles has a higher Nusselt number and friction factor compared to the smooth circular pipe without baffles. Periodically fully developed conditions are obtained after a certain module. Maximum thermal performance factor is obtained for the baffle angle of 150°. Results show that baffle distance, baffle angle, and Reynolds number play important role on both flow and heat transfer characteristics. All the numerical results are correlated within accuracy of ±10% and ±15% for average Nusselt number and Darcy friction factor, respectively.

Key words: *pipe, friction factor, heat transfer, turbulent flow, baffle*

Introduction

Heat transfer from a surface is increased with increasing convection heat transfer coefficient or increasing heat transfer surface area. In order to enhance the heat transfer coefficient, a pump or fan is used, or existing one is replaced with a larger one; however, it may or may not be convenient. Another method to increase the heat transfer from a surface is to increase the surface area. Heat transfer surface area may be increased using baffles or fins on the surfaces of the ducts [1].

Turbulent flows in circular pipes are encountered in many engineering applications such as nuclear reactors, shell and tube heat exchangers, cooling of gas turbines and combustion chambers, and cooling of electronic devices.

Turbulent flow and heat transfer in circular pipes have been studied by a number of investigators. Turbulent flow and heat transfer for tubes and annuli with longitudinal internal fins were analyzed by Patankar *et al*. [2]. Al-Arabi [3] examined the effect of entrance condition on forced convection heat transfer in a tube. El-Sayed *et al*. [4] experimentally investigated to determine the detailed module-by-module pressure drop characteristics of flow inside circular tubes. Lai and Yang [5] numerically investigated turbulence suppression in a pipe. Nieckele and Saboya [6] performed an experimental study to determine average friction factor

* Corresponding author; e-mail: oturgut@gazi.edu.tr

and heat transfer coefficient for flow in pinned annular region of a double-pipe heat exchanger. Akansu [7] numerically studied heat transfer and pressure drop for porous rings inserted in a pipe. Tijing *et al.* [8] investigated the effect of straight and twisted internal fins on heat transfer enhancement. Yucel and Dinler [9] numerically studied 2-D turbulent flow through a pipe with fins attached circumferentially. Tandiroglu and Ayhan [10] experimentally investigated the energy dissipation analysis of transient forced convection heat transfer in a circular duct having baffles inside the duct. Tandiroglu [11, 12] conducted experimental study to investigate the effect of the flow geometry parameters on heat transfer and entropy generation. Dinler and Yucel [13] numerically investigated 2-D turbulent flow and heat transfer in a pipe. Abraham *et al.* [14] numerically investigated heat transfer in pipe. Wang *et al.* [15] numerically investigated the turbulent flow and heat transfer for tubes with longitudinal internal finned tubes. Abraham *et al.* [16] numerically investigated heat transfer for three different duct types. Raj and Ganne [17] numerically studied the effect of shell-side baffle inclination angle on flow and heat transfer. Selvanaj *et al.* [18] carried out a numerical study to study flow and heat transfer in a circular pipe.

A survey of the literature reveals the lack of information on steady-state 3-D forced convection turbulent heat transfer and pressure drop for circular pipes with baffles. In this study, the characteristics of a steady-state 3-D turbulent flow and heat transfer in a circular pipe with nine baffles are investigated numerically using commercial software Ansys Fluent 12.0.1 under constant wall heat flux boundary condition. Standard k-ε turbulence model is used to simulate flow. The effects of Reynolds number, baffle distance, and baffle angle on fluid flow and heat transfer are examined. The results of this investigation are hoped to provide numerical data for 3-D turbulent convective heat transfer in complex geometries.

Description of the physical problem

The geometry, co-ordinate system, computational domain, and characteristics of the circular pipe used in the present study are shown in fig. 1. Computational domain consists of two consecutive parts: a 2.0 m in length entrance section L_1, and a 1.0 m in length test section L_2. To reach the hydrodynamically fully developed conditions at the inlet of the test section, an entrance section is used. The length-to-diameter ratio L_1/D is selected as 64.5 for the entrance section, which is believed to be sufficient to provide hydrodynamically fully developed flow in the entrance section [19]. The length-to-diameter ratio in the test section L_2/D is selected to be 32.3. Both the entrance section and the test section are mathematically modeled separately for numerical computations. The flow is considered to be symmetric with respect to the y-z plane. Hence, only one half of the duct is considered for computational domain

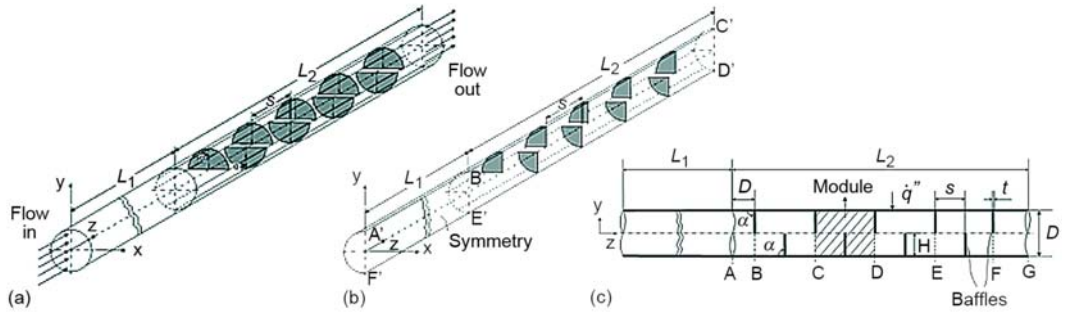

Figure 1. Computational domain; (a) and (b) on *x*-*y*-*z* plane, (c) on *y*-*z* plane

which is shown in fig. 1(b). The principle flow is in the *z*-direction. In fig. 1, *s* is the baffle distance, α – the baffle angle, L_1 – the length of the entrance section, L_2 – the length of the test section, *t* – the baffle thickness, *H* – the baffle height, and *D* – the diameter of the circular pipe. The direction of inclination of baffle angle α is chosen in the flow direction. Shaded area consisting of three baffles shown in fig. 1(c) is called module.

The first baffle is located at one diameter length from the pipe entrance of the test section. Totally nine baffles are placed in the test section. Baffle thickness *t*, pipe diameter *D*, length-to-diameter ratio L_1/D for the entrance section, and length-to-diameter ratio for the test section L_2/D are kept constant at 2 mm, 31 mm, 64.5, and 32.3, respectively. Baffle height-to-diameter ratio H/D is 0.5 for baffle angle of 90°. Baffle height for other baffle angles is so chosen that baffle surface area is kept constant. Five different baffle angles α = 30°, 60°, 90°, 120°, and 150° are considered, and three different baffle distances s/D = 1, 2, and 3 are considered for each baffle angle. For each case, numerical study has been carried out for thirteen different Reynolds numbers between 3000 and 50,000.

Turbulent flow enters the test section with a fully developed velocity profile and constant temperature. The 3-D Navier-Stokes and energy equations are used to describe the flow and heat transfer in the computational domain. The 3-D incompressible Newtonian flow with negligible buoyancy effects and viscous dissipation at steady state has been regarded as turbulent. Thermophysical properties are assumed to be constant. Thus, the governing equations for continuity, momentum, energy, and standard k-ε turbulence model can be written as follows, respectively:

$$\nabla\vec{\mathrm{u}} = 0 \tag{1a}$$

$$\nabla(\rho\vec{\mathrm{u}}\vec{\mathrm{u}}) = -\nabla P + \nabla\boldsymbol{\tau} \tag{1b}$$

$$\nabla(\vec{\mathrm{u}}\rho h) = \nabla(k_{\mathrm{eff}}\nabla T) \tag{1c}$$

$$\frac{\partial}{\partial x_i}\rho u_i k = \frac{\partial}{\partial x_i}\left[\left(\mu + \frac{\mu_t}{\sigma_k}\right)\frac{\partial k}{\partial x_i}\right] + G_k - \rho\varepsilon \tag{1d}$$

$$\frac{\partial}{\partial x_i}(\rho u_i \varepsilon) = \frac{\partial}{\partial x_i}\left[\left(\mu + \frac{\mu_t}{\sigma_\varepsilon}\right)\frac{\partial \varepsilon}{\partial x_i}\right] + \frac{\varepsilon}{k}(\mathrm{c}_1 G_k - \mathrm{c}_2\rho\varepsilon) \tag{1e}$$

where P is the pressure, h – the specific enthalpy, k – the turbulent kinetic energy, and ε – the turbulent dissipation rate. $\boldsymbol{\tau}$ is the stress tensor, k_{eff} – the effective thermal conductivity, μ_{t} – the turbulence viscosity, and G_{k} – the production rate and defined as, respectively:

$$\boldsymbol{\tau} = (\mu + \mu_t)\left[(\nabla\vec{\mathrm{u}} + \nabla\vec{\mathrm{u}}^T) - \frac{2}{3}\nabla\vec{\mathrm{u}}\vec{\mathrm{I}}\right] \tag{2a}$$

$$k_{\mathrm{eff}} = K + \frac{c_{\mathrm{p}}\mu_{\mathrm{t}}}{\mathrm{Pr}_{\mathrm{t}}} \tag{2b}$$

$$\mu_t = c_\mu \rho \frac{k^2}{\varepsilon} \tag{2c}$$

$$G_k = \mu_t \frac{\partial u_i}{\partial x_j}\left(\frac{\partial u_i}{\partial x_j} + \frac{\partial u_j}{\partial x_i}\right) \tag{2d}$$

where K is the thermal conductivity, $\mathrm{Pr_t}$ – the turbulent Prandtl number, and its value is 0.85. Turbulence model constants used: $\sigma_k = 1.0$, $\sigma_\varepsilon = 1.3$, $c_\mu = 0.09$, $c_1 = 1.44$, and $c_2 = 1.92$.

First, the continuity, momentum, and turbulence equations are solved in the entrance section. The fluid enters the entrance section with uniform velocity at $z = 0$, *i. e.*:

$$u = 0, \quad v = 0, \quad w = W_{\mathrm{in}}, \quad k = 0.005\ W_{\mathrm{in}}^2, \quad \varepsilon = \frac{C_\mu k^{1.5}}{0.03R} \tag{3a}$$

No slip boundary conditions are employed on the pipe wall, *i. e.*:

$$u = 0, \quad v = 0, \quad w = 0, \quad k = 0, \quad \frac{\partial \varepsilon}{\partial n} = 0 \tag{3b}$$

where n indicates the direction of the outer normal to the boundary. At the outlet of the entrance section, pressure outlet boundary condition is used. That is, the zero diffusion flux condition for all variables except pressure is implemented at the outlet boundary; gauge pressure is chosen as zero at the outlet. Thus, boundary conditions at the outlet of the entrance section (at $z = L_1$) are given as:

$$\frac{\partial u}{\partial z} = 0, \quad \frac{\partial v}{\partial z} = 0, \quad \frac{\partial w}{\partial z} = 0, \quad \frac{\partial k}{\partial z} = 0, \quad \frac{\partial \varepsilon}{\partial z} = 0 \tag{3c}$$

Symmetry boundary condition is employed on the symmetry plane of the entrance section, A′B′E′F′ plane in fig. 1(b), *i. e.*:

$$u = 0, \quad \frac{\partial v}{\partial x} = 0, \quad \frac{\partial w}{\partial x} = 0, \quad \frac{\partial k}{\partial x} = 0, \quad \frac{\partial \varepsilon}{\partial x} = 0 \tag{3d}$$

Next, the continuity, momentum, energy, and turbulence equations are solved in the test section. The fluid enters the test section with a fully developed velocity profile. The necessary pertinent parameters obtained numerically at the outlet of the entrance section are recorded in a file, and the information within this file is provided as input to the inlet of the test section. The inlet temperature of the fluid is uniform, *i. e.*, $T = T_{\mathrm{in}}$. No slip boundary condition is employed on the duct wall and baffle surfaces. Constant wall heat flux boundary condition is applied to the pipe wall and baffle surfaces as depicted in fig. 1(c), *i. e.*:

$$u = 0, \quad v = 0, \quad w = 0, \quad \frac{\partial T}{\partial n} = \frac{q''}{K}, \quad k = 0, \quad \frac{\partial \varepsilon}{\partial n} = 0 \tag{4a}$$

Symmetry boundary condition is employed on the symmetry plane of the test section, *i. e.*:

$$u = 0, \quad \frac{\partial v}{\partial x} = 0, \quad \frac{\partial w}{\partial x} = 0, \quad \frac{\partial T}{\partial x} = 0, \quad \frac{\partial k}{\partial x} = 0, \quad \frac{\partial \varepsilon}{\partial x} = 0 \tag{4b}$$

The pressure outlet boundary condition is used at the outlet of the test section (at $z = L_1 + L_2$), *i. e.*:

$$\frac{\partial u}{\partial z} = 0, \quad \frac{\partial v}{\partial z} = 0, \quad \frac{\partial w}{\partial z} = 0, \quad \frac{\partial T}{\partial z} = 0, \quad \frac{\partial k}{\partial z} = 0, \quad \frac{\partial \varepsilon}{\partial z} = 0 \tag{4c}$$

Reynolds number Re is defined on the basis of inlet velocity and diameter, *i. e.*,

$$\mathrm{Re} = \frac{\rho W_{\mathrm{in}} D}{\mu} \tag{5}$$

The peripherally averaged local Darcy friction factor f_z and Nusselt number Nu_z for circular pipes are expressed, respectively:

$$f_z = \frac{8\tau_{\mathrm{w},z}}{\rho W_{\mathrm{in}}^2} \tag{6}$$

$$\mathrm{Nu}_z = \frac{\dot{q}''_{\mathrm{w},z} D}{K[T_{\mathrm{w}}(z) - T_{\mathrm{b}}(z)]} \tag{7}$$

In eq. (6), $\tau_{\mathrm{w},z}$ is the peripherally averaged shear stress on the wall at any axial location z. In eq. (7), K is the thermal conductivity, and $\dot{q}''_{\mathrm{w},z}$ is the peripherally averaged heat flux on the wall at any axial location z. $T_{\mathrm{w}}(z)$ and $T_{\mathrm{b}}(z)$ are the wall and bulk temperatures, respectively, at any axial location z. The bulk temperature $T_{\mathrm{b}}(z)$ at an axial location z is calculated:

$$T_{\mathrm{b}}(z) = \int_{A_{\mathrm{c}}} \frac{wT\mathrm{d}A_{\mathrm{c}}}{A_{\mathrm{c}} w_{\mathrm{m}}} \tag{8}$$

where A_{c} is the cross-sectional area, and w_{m} is the mean velocity. The average Nusselt number for the pipe is given as:

$$\mathrm{Nu} = \frac{hD}{K} = \frac{\dot{q}''D}{K(T_{\mathrm{w}} - T_{\mathrm{m}})} \tag{9}$$

where h is the average heat transfer coefficient, $\dot{q}''$ – the average heat flux, T_{w} – the constant wall temperature, and T_{m} – the average bulk temperature of the fluid and defined:

$$T_{\mathrm{m}} = \frac{T_{\mathrm{bi}} + T_{\mathrm{bo}}}{2} \tag{10}$$

where T_{bi} and T_{bo} are the inlet and outlet bulk temperatures. Average Darcy friction factor is given:

$$f = 2\frac{\Delta P}{L}\frac{D}{\rho W_{\mathrm{in}}^2} \tag{11}$$

where ΔP is the pressure drop along the duct, and L – the axial length of the duct. Thermal performance factor η for a given pumping power is defined [20-23]:

$$\eta = \frac{\dfrac{\mathrm{Nu}}{\mathrm{Nu}_{\mathrm{o}}}}{\sqrt[3]{\dfrac{f}{f_{\mathrm{o}}}}} \tag{12}$$

where Nu_{o} and f_{o} are the Nusselt number and friction factor for smooth pipe, respectively. Air is used as the fluid. The physical properties of fluid are taken from Cengel and Ghajar [1] at 290 K.

Numerical solution procedure

Numerical solutions are carried out using Ansys Fluent 12.0.1, a commercial finite-volume-based CFD program. Turbulence is modeled employing the standard k-ε turbulence model with enhanced wall treatment, a near-wall modeling method that unites a two-layer model applicable in regions with fine near wall meshes with enhanced wall functions used in regions with coarse meshes [24]. The Reynolds averaged Navier-Stokes equations are solved numerically in conjunction with transport equations for turbulent flow. Near wall regions are fully resolved for $y^+ < 1.1$ in all the calculations. In the present study, non-uniform tetrahedral grids are employed for all numerical solutions performed. Typical mesh distribution on y-z plane is shown in fig. 2(a) for five different baffle angles. Figure 2(b) shows the typical mesh distribution on *x*-*y*-*z* plane.

The grid independence study is performed by changing the mesh size inside the computational domain until the variation in both Nusselt number and Darcy friction factor are less than 0.4% and 0.9%, respectively. Steady segregated solver is employed with second order upwind scheme for convective terms in the mass, momentum, energy, and turbulence equations. SIMPLE-algorithm has been used for pressure-velocity coupling discretization. To test grid in-

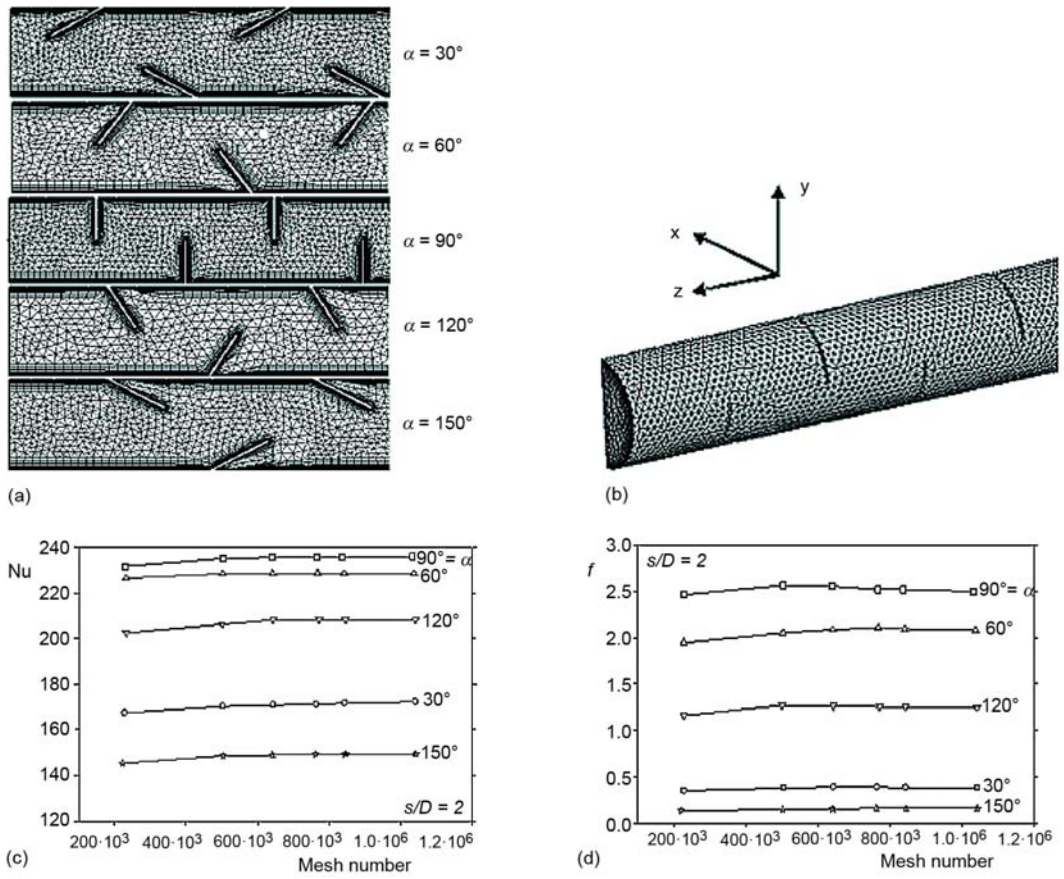

Figure 2. Typical mesh distribution on y-z plane (a), and on x-y-z plane (b) in the computational domain, (c) typical average Nusselt number, and (d) Darcy friction factor *vs.* mesh number

dependence solutions, six different grid sizes changing from 228,951 to 1,033,683 for Re = 50,000 are conducted at $\alpha = 90°$ and $s/D = 2$. It is observed that further refinement of grids from 766,426 to 1,033,683 for Re = 50,000 at $\alpha = 90°$ and $s/D = 2$ did not have a significant effect on the results in terms of average Nusselt number and average Darcy friction factor as shown in fig. 2(c) and 2(d), respectively. Based on this observation, 766,426 mesh size is considered for the final simulation at $\alpha = 90°$ and $s/D = 2$. This grid is also used for other Reynolds numbers at $\alpha = 90°$ and $s/D = 2$. For other baffle angles and baffle distances analyzed here, the optimum mesh size is obtained in a similar manner. Typical average Nusselt number and average Darcy friction factor for other baffle angles are also given in fig. 2(c) and 2(d), respectively, as a function of mesh number. No convergence problems were observed. To acquire convergence, each equation for mass, momentum, and turbulence has been iterated until the residual falls below 10^{-5} whilst energy equation has been iterated until the residual falls below 10^{-6}.

Results and discussion

Validation of numerical method

The fully developed Nusselt numbers and friction factors obtained in the present study for smooth pipe without baffles are compared with those given in the literature. In order to determine whether or not hydrodynamically fully developed flow has been reached at the outlet of the entrance section, the peripherally averaged local Darcy friction factor along pipe is plotted in fig. 3(a). Friction factor is maximum at the pipe entrance, then it decreases with increasing z and approaches a constant value. Friction factor decreases with increasing Reynolds number. Similarly, to determine whether thermally fully developed flow has been reached at the outlet of the test section or not, the peripherally averaged local Nusselt number along the pipe is sketched in fig. 3(b). As can be seen from the figure, local Nusselt number takes maximum value at the beginning of the test section and then decreases until it reaches its asymptotic value. Nusselt number increases with increasing Reynolds number, as expected.

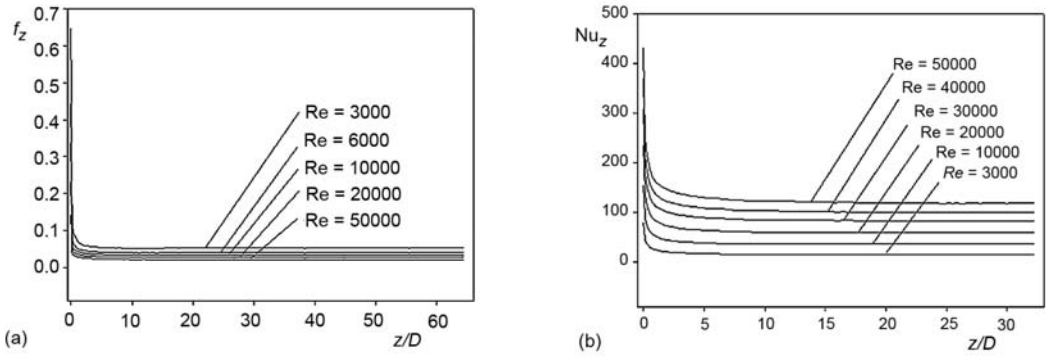

Figure 3. Local Darcy friction factor (a), and local Nusselt number along the test section (b)

For fully developed turbulent flow in circular pipes with smooth surfaces, Nusselt number and Darcy friction factor correlations cited in [1] and [19] are given in tab. 1.

In fig. 4(a), results for fully developed Nusselt number are compared against those of Colburn, Dittus-Boelter, Gnielinski, and Petukhov, eqs. (13)-(16).

On the average, the Nusselt number obtained in this study is about 6.8, 9.3, 17.6, and 19.4% higher than the results obtained from correlations of Colburn, Dittus-Boelter, Gniel-

inski, and Petukhov, eqs. (13)-(16), respectively. Examination of this figure indicates that present results are in agreement with the literature results.

With regard to friction factor, fig. 4(b) presents fully developed Darcy friction factor results of the present study for smooth pipe with the Petukhov, Prandtl, and Blasius correlations, eqs. (17)-(19). On the average, the difference between the Darcy friction factor obtained in this study and the results obtained from correlations of Petukhov, Prandtl, and Blasius is about 8.7, 16.5, and 16.1%, respectively. It is seen that predicted friction factor results show good agreement with previous results.

Table 1. Nu and *f* correlations for fully developed turbulent flow in circular pipes

$\mathrm{Nu} = 0.023\,\mathrm{Re}^{0.8}\,\mathrm{Pr}^{1/3}$	for Re > 10,000	Colburn	(13)
$\mathrm{Nu} = 0.023\,\mathrm{Re}^{0.8}\,\mathrm{Pr}^{0.4}$	for Re > 10,000	Dittus--Boelter	(14)
$\mathrm{Nu} = \dfrac{(f/8)(\mathrm{Re}-1000)\,\mathrm{Pr}}{1+12.7(f/8)^{0.5}(\mathrm{Pr}^{2/3}-1)}$	for $3\cdot10^3 < \mathrm{Re} < 5\cdot10^6$	Gnielinski	(15)
$\mathrm{Nu} = \dfrac{(f/8)\,\mathrm{Re}\,\mathrm{Pr}}{1.07+12.7(f/8)^{0.5}(\mathrm{Pr}^{2/3}-1)}$	for $10^4 < \mathrm{Re} < 5\cdot10^6$	Petukhov	(16)
$f = (0.790\,\ln\mathrm{Re} - 1.64)^{-2}$	for $3\cdot10^3 < \mathrm{Re} < 5\cdot10^6$	Petukhov	(17)
$1/f^{0.5} = 2.0\,\log(\mathrm{Re}\,f^{0.5}) - 0.8$	for Re > 4000	Prandtl	(18)
$f = 0.316\,\mathrm{Re}^{-0.25}$	for $4000 < \mathrm{Re} < 10^5$	Blasius	(19)

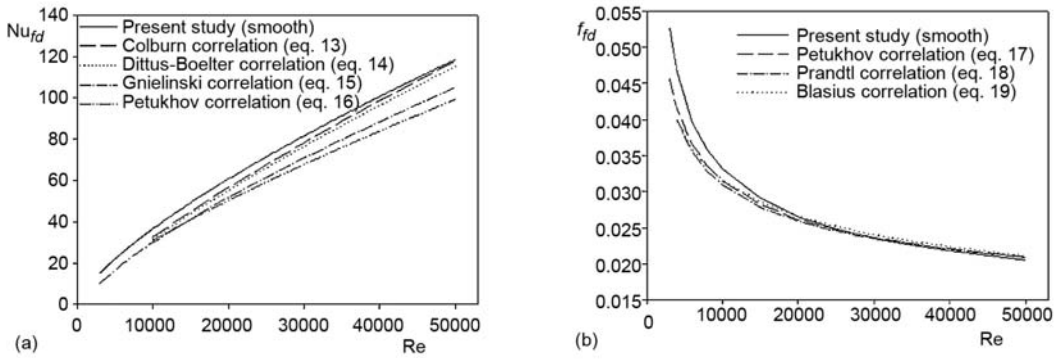

Figure 4. Variation of fully developed Nusselt number (a) and friction factor (b) with Reynolds number

Results for circular pipe with baffle

Typical variation of average Nusselt number with Reynolds number is presented in fig. 5(a) for baffle distance of $s/D = 2$. The results of smooth pipe are also given in fig. 5(a). Nusselt number for a pipe with baffles is greater than the Nusselt number for smooth pipe. Baffle angle of $\alpha = 90°$ provides maximum Nusselt number while baffle angle of $\alpha = 150°$ gives minimum Nusselt number. As can be seen in fig. 5(a), heat transfer depends on the baffle angle especially at high Reynolds numbers. Nusselt number increases with increasing α from 30 to 90°, and takes its maximum value at $\alpha = 90°$, and then Nusselt number begins to decrease with

increasing α from 90 to 150°. In other words, Nusselt number increases by 38% while baffle angle changes from 30 to 90°, and Nusselt number decreases by 37% while baffle angle increases from 90 to 150°. Similar results are seen for other baffle distances. However, these results are omitted due to page limit. It is seen that Nusselt number is between 1.3 and 2.3 times the smooth pipe. In fig. 5(b), the average Nusselt number is plotted as a function of Reynolds number to study the effects of baffle distance on heat transfer for α = 90°. It is seen that the average Nusselt number increases with increasing Reynolds number and baffle distance in the range studied. The results of smooth pipe are presented in fig. 5(b) as well. It is seen that heat transfer obtained for three baffle distances *s*/*D* = 1, 2, and 3 is higher than that of smooth pipe.

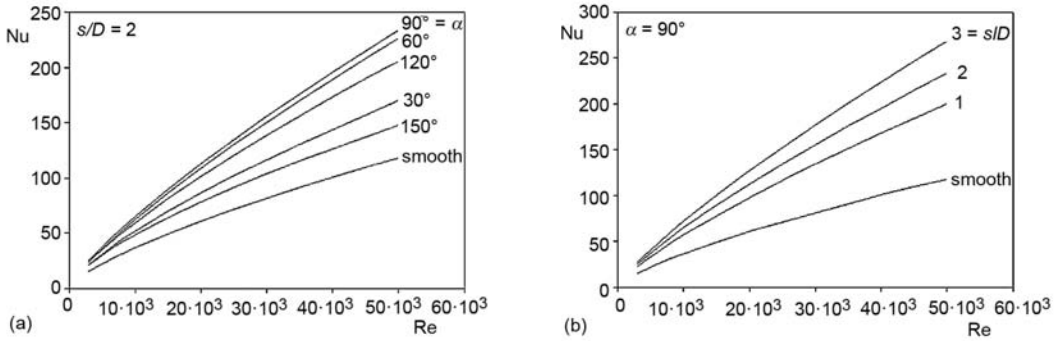

Figure 5. Effect of baffle angle (a) and baffle distance (b) on heat transfer

Typical average Nusselt numbers for each module along pipe at α = 90° for Re = 3000 and 50,000 are presented in fig. 6 for two baffle distances *s*/*D* = 1 and 3. The horizontal lines point out the distance for each module length. Figure 6 shows a difference of 1.3% between the average of the fourth module and third module for Re = 3000 when *s*/*D* = 1. Likewise, the difference between the average of the fourth module and third module for Re = 50,000 when *s*/*D* = 1 is 1.15%. Thus, it can be said that periodically fully developed flow occurs after second module for Re = 3000 and 50,000 when *s*/*D* = 1. It is also seen that periodically fully developed flow occurs after second module for baffle distances of *s*/*D* = 2 and 3 for Re = 3000 and 50,000.

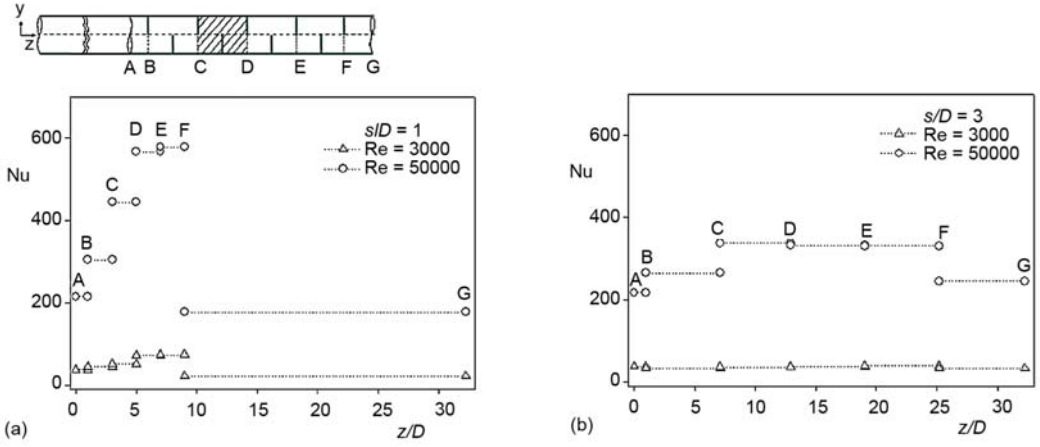

Figure 6. Typical variation of average Nusselt number along pipe with α = 90°

To show the effect of baffle angle on pressure loss, typical variation of average Darcy friction factor with Reynolds number for baffle distance $s/D = 2$ is presented in fig. 7(a). Smooth pipe results are also presented in fig. 7(a).

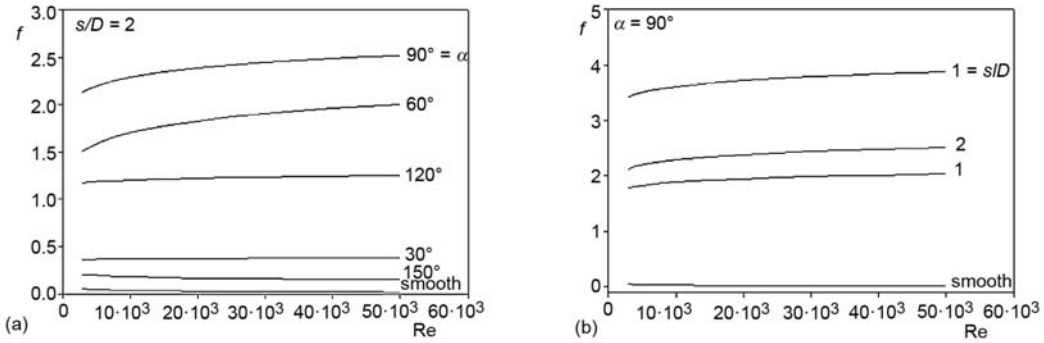

Figure 7. Effect of baffle angle (a), and baffle distance (b) on pressure loss

It is seen that pressure loss depends on the baffle angle; baffle angle of $\alpha = 90°$ gives maximum pressure loss while baffle angle of $\alpha = 150°$ provides minimum pressure loss for three baffle distances. In other words, the resistance to the flow due to baffles is maximum and minimum at 90° and 150°, respectively; therefore, friction factor is maximum and minimum at 90° and 150°, respectively. As can be seen from fig. 7(a), friction factor increases with increasing Reynolds number except $\alpha = 150°$ for which friction factor decreases due to decrease in friction losses. Similar results are seen for other baffle distances $s/D = 1$ and 3. It is seen that friction factor for baffled duct increases between 4.1 and 179.5 times the smooth pipe values. The effect of baffle distance on pressure loss is presented in fig. 7(b) for $\alpha = 90°$. Examination of fig. 7(b) shows that pressure loss in the circular pipe with baffle depends on the baffle distance. At constant Reynolds number, the resistance to the flow due to baffles decreases with increasing baffle distance s/D; thus, friction factor decreases with increasing baffle distance in the range studied. However, friction factor increases with increasing Reynolds number. Similar results are seen for other baffle angles.

Typical dimensionless axial velocity w/W_{in} profiles on the symmetry plane, B′C′D′E′ plane, see fig. 1(b), are plotted in fig. 8 at different locations along pipe when $s/D = 1$ and $\alpha = 90°$ for Re = 50,000. Axial velocity values are scaled to the inlet velocity. The figure on the left side shows the dimensionless axial velocity profiles along lines of A″B″, C″D″, E″F″, and G″H″ shown in fig. 8, at the middle of the two baffles in the first half of the modules, for Re = 50,000. The figure on the right side indicates the dimensionless axial velocity profiles along lines of A‴B‴, C‴D‴, E‴F‴, and G‴H‴ shown in fig. 8, at the middle of the two baffles in the second half of the modules, for Re = 50,000. As will be seen from fig. 8, the velocity profiles in third and fourth modules, *i. e.* along lines of E″F″ and G″H″, and E‴F‴and G‴H‴, are almost same. In other words, flow approaches periodically fully developed conditions at third module. The negative velocities point out the presence of recirculation behind the baffles. It can be seen in fig. 8*a* that velocity increases in the lower half of the pipe due to baffle placed in the higher part of the duct, and reverse flow occurs in the higher part of the pipe. Regarding fig. 8(b), velocity increases in the higher part of the pipe due to baffle placed in the lower part of the pipe, and reverse flow happens in the lower part of the pipe. As can be seen in fig. 8, the velocity at wall is zero due to no-slip boundary conditions which are used in this study.

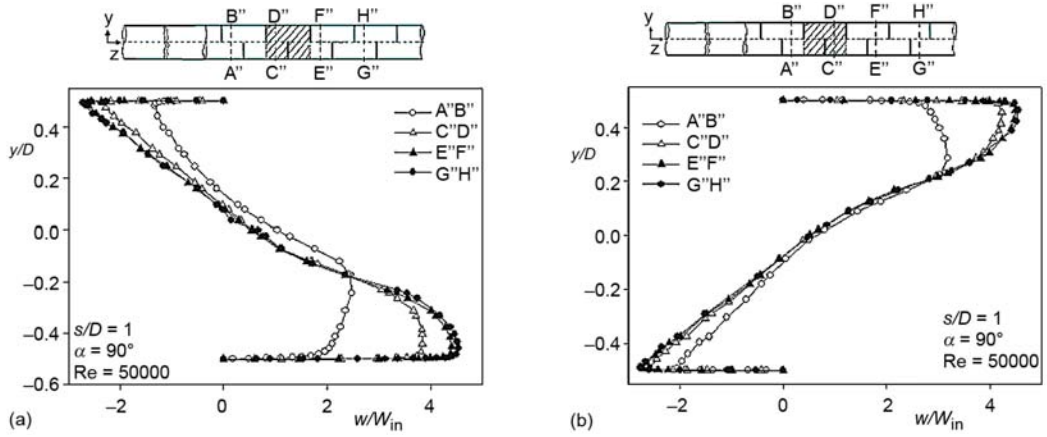

Figure 8. Typical dimensionless axial velocity profiles on the symmetry plane in the first and second half of the modules for Re = 50,000

In fig. 9, dimensionless axial velocity profiles w/W_{in} on the symmetry plane, B′C′D′E′ plane, see fig. 1(b), are plotted along line G″H″ shown in fig. 9, at the middle of the two baffles in the first half of the fourth module (last module), at three different baffle distances when $\alpha = 90°$ and Re = 3000. It is seen that the magnitude of dimensionless axial velocity increases with decreasing baffle distance. It is also seen that the intensity of reverse flow increases with decreasing baffle distance, so reverse flow with high intensity results in high pressure loss and high friction factor.

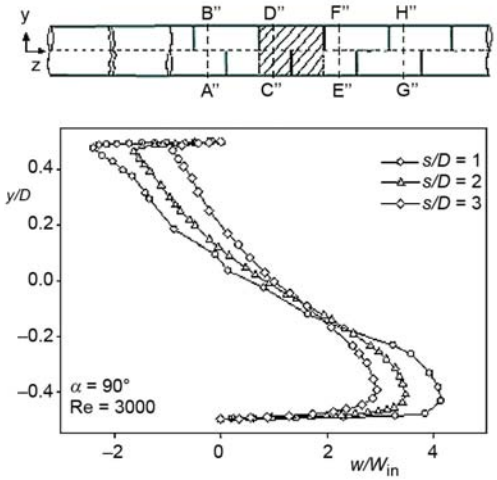

Figure 9. Typical dimensionless axial velocity profiles on the symmetry plane along line G″H″, in the first half of the fourth module, for three different baffle distances

Typical average Darcy friction factor for each module along pipe at $\alpha = 90°$ for Re = 3000 and 50,000 are presented in fig. 10 for baffle distances of $s/D = 1$ and 3. The horizontal lines indicate the distance for each module length. Figure 10 shows a difference of 2.2% between the average of the fourth and third module for Re = 3000 when $s/D = 1$. Likewise, the difference between the average of the fourth and third module for Re = 50,000 when $s/D = 1$ is 2.4%. Hence, it can be said that periodically fully developed flow occurs after second module for Re = 3000 and 50,000 when $s/D = 1$. Velocity profiles presented in fig. 8 also supports these results. It is also seen that periodically fully developed flow occurs after second module for baffle distances of $s/D = 2$ and 3 for Re = 3000 and 50,000.

Typical stream line contours are given in fig. 11 for three different baffle angles at $s/D = 2$ and Re = 10,000. It is seen that the presence of the baffles which are placed in the lower half of the pipe cause a reduction of velocity in this region while they cause an increase in the flow in the higher half of the pipe. As can be seen in fig. 11, re-circulation occurs after baffles. Maximum velocity is obtained for $\alpha = 90°$ due to decreasing flow passage area.

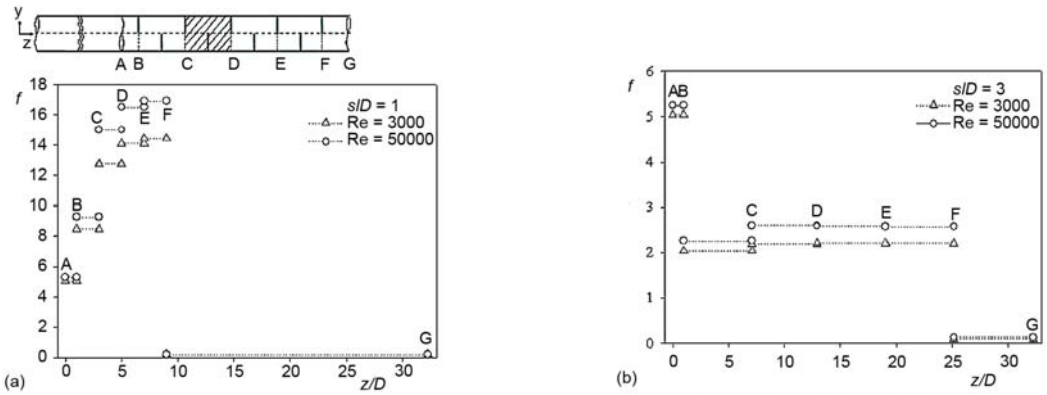

Figure 10. Typical variation of average friction factor along pipe with $\alpha = 90°$

Typical stream line contours are given in fig. 12 for three different baffle distances (s/D = 1, 2 and 3) at $\alpha = 90°$ and Re = 10,000. It is seen that reverse flow occurs after the baffles; negative values on the scale indicate the reverse flow. It is also seen that velocity increases due to small passage area while the distance between two baffles decreases.

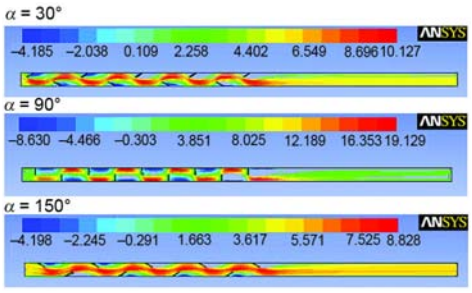

Figure 11. Variation of streamlines along the pipe for three different α at s/D = 2 and Re = 10,000
(for color image see journal web-site)

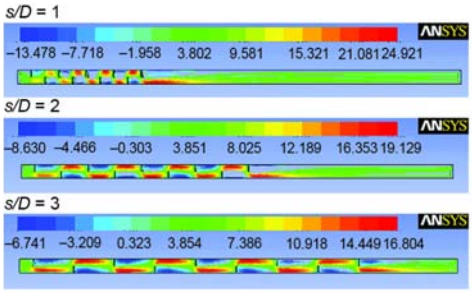

Figure 12. Variation of streamlines along the pipe for three different s/D at $\alpha = 90°$ and Re = 10,000
(for color image see journal web-site)

Equations are obtained with least square method in the form of $\mathrm{Nu} = a\mathrm{Re}^b(s/D)^c$ and $f = a\mathrm{Re}^b(s/D)^c$ for average Nusselt number and Darcy friction factor, respectively. The values of a, b, and c are given in tab. 2 for average Nusselt number and Darcy friction factor. A general equation is also given in tab. 2 for each baffle angle. Correlations given in tab. 2 for s/D = 1, 2, and 3 represent the numerical data within ±0.7% for Darcy friction factor and ±1.3% for Nusselt number. General correlations given in tab. 2 for each baffle angle represent the numerical data within ±8.1% for Darcy friction factor and ±4.1% for Nusselt number.

In order to provide a single equation for average Darcy friction factor and Nusselt number representing all numerical results, the variation of average Darcy friction factor f and Nusselt number Nu as a function of Reynolds number Re, baffle spacing s/D, and baffle angle α are expressed, respectively:

$$f = 2.294\,\mathrm{Re}^{0.017}\left(\frac{s}{D}\right)^{-0.460}\mathrm{Pr}^{0.4}\left(\frac{A_b}{A_o}\right)\left[1.749 - 29.63\left(\frac{\alpha}{180}\right) + \right.$$
$$\left. +177.9\left(\frac{\alpha}{180}\right)^2 - 312.4\left(\frac{\alpha}{180}\right)^3 + 166.7\left(\frac{\alpha}{180}\right)^4\right] \tag{20}$$

$$\mathrm{Nu} = 2.294\,\mathrm{Re}^{0.759}\left(\frac{s}{D}\right)^{0.167}\mathrm{Pr}^{0.4}\left(\frac{A_b}{A_o}\right)\left[0.021 + 0.153\left(\frac{\alpha}{180}\right) - \right.$$
$$\left. -0.184\left(\frac{\alpha}{180}\right)^2 + 0.011\left(\frac{\alpha}{180}\right)^3 + 0.022\left(\frac{\alpha}{180}\right)^4\right] \quad (21)$$

Table 2. Correlation constants for Nusselt number and Darcy friction factor

α	s/D	$\mathrm{Nu} = a\mathrm{Re}^b(s/D)^c$			$f = a\mathrm{Re}^b(s/D)^c$		
		a	b	c	a	b	c
30°	1	0.056	0.734	0	0.379	0.029	0
	2	0.059	0.736	0	0.326	0.014	0
	3	0.062	0.736	0	0.404	0.003	0
	General	0.055	0.735	0.120	0.429	0.015	–0.357
60°	1	0.044	0.775	0	1.180	0.111	0
	2	0.040	0.799	0	0.669	0.102	0
	3	0.038	0.816	0	0.770	0.065	0
	General	0.036	0.797	0.216	1.397	0.093	–0.856
90°	1	0.045	0.776	0	2.418	0.044	0
	2	0.045	0.791	0	1.334	0.059	0
	3	0.040	0.815	0	1.220	0.047	0
	General	0.037	0.794	0.239	2.260	0.050	–0.605
120°	1	0.047	0.765	0	1.304	0.016	0
	2	0.049	0.771	0	0.968	0.024	0
	3	0.046	0.787	0	0.913	0.021	0
	General	0.042	0.774	0.190	1.243	0.020	–0.287
150°	1	0.072	0.701	0	0.380	-0.061	0
	2	0.085	0.690	0	0.479	-0.107	0
	3	0.085	0.691	0	0.453	-0.099	0
	General	0.077	0.694	0.065	0.492	-0.089	–0.201

In eqs. (20) and (21), α is the baffle angle, $A_b = A_o/2$ is the one surface area of the baffle, and A_o is the smooth channel cross-sectional area. Equation (20) provides the results within ±15% for 83% of the numerical data and within ±20% for 91% of the numerical data while eq. (21) gives the results within ±10% for 97% of the numerical data. Equations (20) and (21) represent the numerical results for $30° \le \alpha \le 150°$, $1 \le (s/D) \le 3$, $3000 \le \mathrm{Re} \le 50{,}000$, $A_b/A_o = 0.5$, and $\mathrm{Pr} = 0.71$.

The given results show that heat transfer rate increases when baffles are used inside pipe; however, the baffle placed inside pipe increases the resistance to the flow and ends up with an increase in the friction factor. For this reason, the values of Nusselt number and friction factor are compared at the same pumping power in fig. 13. Figure 13(a) presents the

thermal performance factor η as a function of Reynolds number at baffle distance of $s/D = 2$. As can be seen from fig. 13(a), the thermal performance factor decreases with increasing Reynolds number. The circular pipe with $\alpha = 150°$ gives the highest thermal performance factor while the circular pipe with $\alpha = 90°$ provides the lowest thermal performance factor. As can also be seen in fig. 13(a), the thermal performance factor is less than unity for all baffle angles. In other words, fluid friction dominates the heat transfer. It is also seen that the thermal performance factor changes between 0.28 and 0.97 depending on the baffle distance and Reynolds number. It can be said that using baffles in a circular pipe in turbulent flow is not advantageous due to low thermal performance factor η which is less than unity.

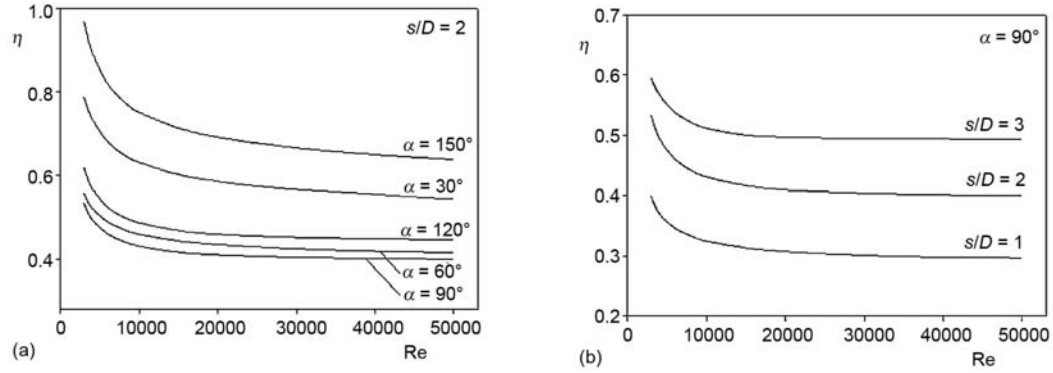

Figure 13. Typical variation of thermal performance factor with Reynolds number for (a) five different baffle angles at $s/D = 2$ and (b) three different baffle distances at $\alpha = 90°$

Variation of thermal performance factor with Reynolds number is presented in fig. 13(b) at $\alpha = 90°$. As can be seen in fig. 13(b), that the thermal performance factor increases with increasing baffle distance in the range of studied at constant Reynolds number. In other words, the lowest pressure penalty is obtained for $s/D = 3$ in the range studied. Therefore, the thermal performance factor of the pipe with $s/D = 3$ is better than the pipes with $s/D = 1$ and 2. In contrast, the highest pressure penalty is obtained for $s/D = 1$, so the lowest thermal performance factor is obtained for pipe with $s/D = 1$. In other words, it is seen from performance analysis that the fluid friction much more dominates the heat transfer as baffle distance s/D decreases. Similar results are seen for other baffle angles.

Conclusions

In this study, the effect of baffles which are attached to the inner surface of a pipe is numerically examined for steady-state 3-D turbulent flow under constant heat flux boundary condition. Nine baffles are attached inside pipe. The parameters examined are the distance between two baffles s, baffle angle α, and Reynolds number. Numerical study has been carried out for the ratio of the baffle distance to the pipe diameter in the range of $s/D = 1$ to 3, baffle angle of $\alpha = 30°$ to 150°, Reynolds number of Re = 3000 to 50,000, and Prandtl number of Pr = 0.71. The values of fully developed Nusselt numbers and Darcy friction factors obtained in the present study for smooth pipe without baffle are compared to those given in the literature to validate the accuracy of the turbulence model and numerical method. It is seen that heat transfer and pressure losses are higher for pipes with baffles. It is also seen that heat transfer, pressure loss, and thermal performance factor for a pipe with baffles depend on the Reynolds number, baffle angle, and distance between two baffles. The use of baffles results in a heat

transfer increment as high as 130% compared with the heat transfer in the smooth pipe. It is also seen that heat transfer increases with increasing Reynolds number and baffle distance in the range studied. Maximum and minimum heat transfers are obtained at α = 90° and 150°, respectively, for all baffle distances. Friction factor increases with increasing Reynolds number except 150° for which friction factor decreases due to decrease in friction losses, and friction factor decreases with increasing baffle distance in the range studied. Pipes with α = 90° and 150°, respectively, give maximum and minimum pressure losses for all baffle distances. New engineering correlations are presented for the Nusselt number and Darcy friction factor. All the numerical data are correlated with ±10 and ±15% error for Nusselt number and Darcy friction factor, respectively. It is seen that thermal performance factor η decreases with increasing Reynolds number but increases with increasing baffle distance in the range studied. Maximum thermal performance factor is obtained at α = 150° while minimum thermal performance factor is obtained at α = 90°. It is also seen that after a certain module, the flow characteristics indicate periodically repeating behavior.

Acknowledgments

The present work is financially supported by the Unit of Scientific Research Projects of Gazi University under the project BAP 06/2010-59.

References

[1] Cengel, Y. A., Ghajar, A. J., *Heat and Mass Transfer Fundamentals and Applications*, McGraw Hill, New York, USA, 2011
[2] Patankar, S. V., *et al*., Analysis of Turbulent Flow and Heat Transfer in Internally Finned Tubes and Annuli, *ASME Journal of Heat Transfer, 101* (1979), 1, pp. 29-37
[3] Al-Arabi, M., Turbulent Heat Transfer in the Entrance Region of a Tube, *Heat Transfer Engineering, 3* (1982), 3-4, pp. 76-83
[4] El-Sayed, S. A., *et al*., Experimental Study of Turbulent Flow Inside a Circular Tube with Longitudinal Interrupted Fins in the Streamwise Direction, *Experimental Thermal and Fluid Science, 15* (1997), 1, pp. 1-15
[5] Lai, J. C. S., Yang, C. Y., Numerical Simulation of Turbulence Suppression: Comparisons of the Performance of Four *k-ε* Turbulence Models, *International Journal of Heat and Fluid Flow, 18* (1997), 6, pp. 575-584
[6] Nieckele, A. O., Saboya, F. E. M., Turbulent Heat Transfer and Pressure Drop in Pinned Annular Regions, *Journal of the Brazilian Society of Mechanical Sciences, 22* (2000), 1, pp. 119-132
[7] Akansu, S. O., Heat Transfers and Pressure Drops for Porous-Ring Turbulators in a Circular Pipe, *Applied Energy, 83* (2006), 3, pp. 280-298
[8] Tijing, L. D., *et al*., A Study on Heat Transfer Enhancement Using Straight and Twisted Internal Fin Inserts, *International Communications in Heat and Mass Transfer, 33* (2006), 1, pp. 719-726
[9] Yucel, N., Dinler, N., Numerical Study of Laminar and Turbulent Flow Through a Pipe with Fins Attached, *Numerical Heat Transfer Part A, 49* (2006), 2, pp. 195-214
[10] Tandiroglu, A., Ayhan, T., Energy Dissipation Analysis of Transient Heat Transfer for Turbulent Flow in a Circular Tube with Baffle Inserts, *Applied Thermal Engineering, 26* (2006), 2-3, pp. 178-185
[11] Tandiroglu, A., Effect of Flow Geometry Parameters on Transient Heat Transfer for Turbulent Flow in a Circular Tube with Baffle Inserts, *International Journal of Heat and Mass Transfer, 49* (2006), 9-10, pp. 1559-1567
[12] Tandiroglu, A., Effect of Flow Geometry Parameters on Transient Entropy Generation for Turbulent Flow in a Circular Tube with Baffle Inserts, *Energy Conversion and Management, 48* (2007), 3, pp. 898-906
[13] Dinler, N., Yucel, N., Flow and Heat Transfer in a Pipe with a Fin Attached to Inner Wall, *Heat and Mass Transfer, 43* (2007), 8, pp. 817-825
[14] Abraham, J. P., *et al*., Heat Transfer in all Pipe Flow Regimes: Laminar, Transitional/Intermittent, and Turbulent, *International Journal of Heat and Mass Transfer, 52* (2009), 3-4, pp. 557-563

[15] Wang, Q. W., *et al*., Effect of Lateral Fin Profiles on Turbulent Flow and Heat Transfer Performance of Internally Finned Tubes, *Applied Thermal Engineering*, *29* (2009), 14-15, pp. 3006-3013
[16] Abraham, J. P., *et al*., Internal Flow Nusselt Numbers for the Low-Reynolds-Number End of the Laminar-to-Turbulent Transition Regime, *International Journal of Heat and Mass Transfer*, *54* (2011), 1-3, pp. 584-588
[17] Raj, R. T. K., Ganne, S., Shell Side Numerical Analysis of a Shell and Tube Heat Exchanger Considering the Effects of Baffle Inclination on Fluid Flow, *Thermal Science*, *16* (2012), 4, pp. 1165-1174
[18] Selvanaj, P., *et al*., Computational Fluid Dynamics Analysis on Heat Transfer and Friction Factor Characteristics of a Turbulent Flow for Internally Grooved Tubes, *Thermal Science*, *17* (2013), 4, pp. 1125-1137
[19] White, F. M., *Fluid Mechanics*, McGraw Hill, New York, USA, 2008
[20] Valencia, A., *et al*., Numerical Study of the Unsteady Flow and Heat Transfer in Channels with Periodically Mounted Square Bars, *Heat and Mass Transfer*, *37* (2001), 2-3, pp. 265-270
[21] Kore, S. S., *et al*., Experimental Investigations of Heat Transfer Enhancement from Dimpled Surface in a Channel, *International Journal of Engineering Science and Technology*, *3* (2011), 8, pp. 6227-6234
[22] Promvonge, P., *et al*., Numerical Heat Transfer Study of Turbulent Square-Duct Flow Through Inline V-Shaped Discrete Ribs, *International Communications in Heat and Mass Transfer*, *38* (2011), 10, pp. 1392-1399
[23] Potdar, U., *et al*., Study of Heat Transfer Coefficient & Friction Factor of Stationary Square Channel with V Shaped 45° Angled Arc of Circle Ribs with Different Blokage Ratio, *International Journal of Applied Sciences and Engineering Research*, *1* (2012), 2, pp. 47-56
[24] ***, Ansys Inc. Fluent 12.0 User's Guide, Lebanon, USA, 2008

Paper submitted: October 11, 2012
Paper revised: March 30, 2014
Paper accepted: April 11, 2014